PCCP

Accepted Manuscript

ROYAL SOCIETY OF CHEMISTRY

www.rsc.org/pccp

Journal Name

ARTICLE TYPE

Cite this: DOI: 10.1039/xxxxxxxxxx

Received Date
Accepted Date

DOI: 10.1039/xxxxxxxxxx

www.rsc.org/journalname

The making of ring currents†

Guglielmo Monaco* and Riccardo Zanasi*

Benzene, planar cyclooctatetraene, and borazine have been taken into account as archetypal aromatic, anti-aromatic, and non-aromatic systems. Then, the making of the π-electron diatropic ring current of benzene, huge paratropic ring current of planar cyclooctatetraene, and weak diatropic ring current of borazine, has been monitored by means of DFT calculations of current density maps and bond current strengths along a concerted, highly symmetric reaction pathway for the trimerization and tetramerization of acetylene to benzene and planar cyclooctatetraene and the trimerization of the simplest iminoborane (BH_2N) to borazine. Besides, a simple model is presented that permits to infer the presence of a ring current only on account of the sum of homotropic local vortices. The model works satisfactorily for borazine and surely as well for benzene with a substantial difference. On the one hand, for borazine, the evolution of the current density along the formation reaction can be recast summing three virtually unchanged diatropic current loops with respect to parent iminoborane molecules. On the other hand, the benzene ring current is an emerging property that can be re-elaborated as the sum of three diatropic current loops of increased diatropicity with respect to parent acetylene molecules, i.e., the radius of the maximum current increases form 0.76 to 0.97 Å and the current strength increases from 3.6 to 6.7 nA T^{-1}. In these terms, the difference between the aromatic benzene and non-aromatic borazine can be understood as the attitude of the acetylene molecules to form always wider and stronger current loops as they get closer, a behavior not shared by the iminoborane molecules. For planar cyclooctatetraene, the paratropic circulation arising from the HOMO-LUMO transition makes the model inapplicable, since the initial hypothesis of homotropic circulations over the reaction coordinate is violated. In a sense, the fact that the model works only for a bit of the planar cyclooctatetraene formation reaction is itself distinctive of the anti-aromatic magnetic response.

1 Introduction

Nearly eighty years ago, and about seventy years after the publication of the celebrated Kekulé's benzene structure,[1] Linus Pauling,[2] Kathleen Lonsdale,[3] and Fritz London[4] proposed the ring current model (RCM) to explain the peculiar magnetic properties of aromatic molecules. The RCM was conceived "on the basis of the assumption that the $2p_z$ electrons (one per aromatic carbon atom) are free to move from carbon atom to adjacent carbon atom under the influence of the impressed fields".[2] The idea that certain electrons can move in this way is implicit in the theory of molecular orbitals, as applied by Hückel to aromatic and unsaturated molecules,[5–8] and is consistent with the idea of electron delocalisation that is a common feature of any aromatic system.

Despite its old age, the RCM has recently received new vigour thanks to the availability of powerful methods for computing the magnetic shieldings in any point of the molecular space. This pointwise approach to compute magnetic shieldings has provided the basis to formulate a number of variations on the RCM theme.[9–16] Beside the RCM, the idea to develop magnetic criteria for aromaticity, in parallel to the introduction of methods for computing, visualizing and interpreting the magnetically induced current density, represent all together an active field of research, as documented in a number of less and more recent reviews on these subjects.[17–22]

According to a common tenet, the presence of a delocalised diatropic (paratropic) current is considered a good aromaticity (anti-aromaticity) indicator.[23–25] Nonetheless, strong delocalised electron currents in noncyclic molecules have been reported.[26,27] Furthermore, delocalised currents are found flowing around weakly interacting molecules, as in the case of hydrogen bonded systems.[28,29] Therefore, the appearance of a delocalised current under the influence of an imposed magnetic field does not

Department of Chemistry and Biology "A. Zambelli", University of Salerno, via Giovanni Paolo II 132, 84084 Fisciano, Italy. Fax: +39 089 969603; E-mail: gmonaco@unisa.it, rzanasi@unisa.it

† Electronic Supplementary Information (ESI) available: animations showing the magnetically induced π-electron current density along reaction coordinates; bond lengths and angles are also provided with Z-matrices for the calculations. See DOI: 10.1039/b000000x/

seem to be an exclusive response of aromatic (anti-aromatic) systems. To clarify better the point, a distinction should be made between the case where only one pure delocalised current is present and the case in which one delocalised current encloses several other circulations. In the latter case, there is some evidence that the actual circulation field is the result of the sum of individual circulations localised around more or less strongly interacting molecular fragments.[30] Then, what is the difference between the two cases? Are they really caused by different phenomena? Is there any implication with the aromaticity concept?

In an attempt to answer to these and other questions that might arise, we have found interesting to consider formation reactions of some archetypal aromatic, anti-aromatic, and non-aromatic systems, in terms of trimerization of acetylene to benzene

$$3C_2H_2 \longrightarrow C_6H_6, \quad (1)$$

tetramerization of acetylene to planar cyclooctatetraene

$$4C_2H_2 \longrightarrow C_8H_8, \quad (2)$$

and trimerization of the simplest iminoborane HBNH (isoelectronic with acetylene)[31] to borazine

$$3BH_2N \longrightarrow B_3H_6N_3, \quad (3)$$

and to study them *in silico* allowing for a hypothetical concerted reaction pathway from isolated acetylene, or iminoborane, molecules to final products. Actually, the effective oligomerizations of acetylene to benzene and iminoborane to borazine proceed with a different mechanism. Although rather ineffective, the classical thermal transformation of acetylene to benzene is a very well known process, whilst borazines are the normal products of thermal stabilization of iminoboranes.[32] Synthesis of COT was reported in 1911 by Willstätter and Waser.[33]

Our choice of the hypotetical concerted oligomerizations 1-3, (see later for details) is a convenient one for our purposes. In this way, the current density, induced at first-order by a perpendicular magnetic field in the π-electrons of the reacting systems, can be monitored from an initial state of isolated molecules, for which the sum of local current densities of individual non interacting fragments is effective, to final products characterized by their respective current flows, i.e., diatropic ring current for benzene, paratropic ring current for planar COT and weakly diatropic ring current for borazine.[23,24,34–36] The idea is that of capturing and quantifying the most important steps of the current transition from local to non local regimes. These information have been obtained and are analysed in section 4 with the help of a simple model for the sum of pure rotational fields specifically introduced in section 3. In summary, this paper is aimed at giving a different point of view about ring currents by looking behind the scene of their formation.

2 Calculation methods

Chemical reactions 1-3 have been studied *in silico* along a concerted, highly symmetric hypothetical reaction pathway. All the reacting acetylene, or iminoborane, molecules have been thought to approach one to each other starting, moving, and distorting simultaneously on the same plane of symmetry, keeping the highest possible symmetry point group, i.e., D_{3h}, D_{4h}, and C_{3h} for reactions 1, 2, and 3 respectively. This leads to a convenient choice for the reaction coordinate (RC) that has been defined as the distance between the centre of symmetry of the whole system and the C≡C, or B≡N, bonds of the reacting units. Then, for each given RC value, equilibrium geometries for the nuclei of the reacting molecules have been obtained by means of the partial optimization procedure available with the Gaussian 09 suite of programs[37] at the density functional theory (DFT) level, using the B97-2 functional[38] and the cc-pVTZ basis set.[39] A detailed description of the Z-matrices used for the geometry optimizations is given within the electronic supplementary information (ESI). Extended tabulations of bond lengths, bond angles, and energies are also provided within the ESI.

2.1 Current density calculation

First-order current densities and related magnetic properties were computed by the CTOCD-DZ2 method[40–44] at DFT level,[45–47] using the SYSMO package[48] and adopting the same combination of functional and basis set used for optimizing the structures. The advantages of the CTOCD method for calculation of currents are well documented.[49] As shown by Flaig and coworkers,[50] benchmarking hydrogen and carbon NMR chemical shifts, the B97-2 functional provides accurate magnetic properties. Moreover, B97-2 molecular structures have been found to be comparable to those obtained using other quite popular functionals.[38]

Within the orbital approximation, the first-order current density induced by a magnetic field in the electrons of a molecule can be formally partitioned into orbital contributions.[51] Since for in plane symmetric molecules, in the presence of a perpendicular magnetic field, π and σ orbitals are symmetry distinct, the total CTOCD-DZ2 current density is readily partitioned into origin independent π and σ contributions.[52] Then, if not otherwise specified, current density maps reported in this work are for the π-electrons perturbed by a perpendicular unitary magnetic field. Maps have been computed pointwise over a plane parallel to the plane of symmetry and above it at the conventional distance of 1 a.u.. Bold (or fat) arrows have been used to represent the current density, with the assumption that arrow surfaces are proportional to the magnitude of the vector over the plotting plane.

2.2 Phase portrait calculation

Critical points are defined as those places where the current density vanishes. Their position and nature allows a detailed analysis of the current density. Two kind of critical points are diffusely encountered that are referred to as centres and saddles.[53] Field trajectories asymptotic to saddles are known as separatrices of the current density and, all together, constitute the so called "phase portrait", which provides a compact and quite useful representation of the basic circulations forming the vector field.[27,30] In particular, a phase portrait permits to quickly separate domains of local circulation from those containing delocalised currents as, for example, the ring current. A Newton-

Raphson based method has been used for the search of the singularities. Critical points have been represented in the current density maps as: green/red dots for centres of diatropic/paraptropic (clockwise/counterclockwise) circulations; blue crosses for saddles, whose arms indicate the orientation of the asymptotic trajectories passing across the saddles. Phase portrait have been worked out by plotting as black continuous lines the separatrices of the current density. A fourth-order Runge-Kutta based method has been used to compute the separatrices by stepwise integration of the vector field.

2.3 Bond current strength calculation

In order to provide a quantification of current fields, bond current strengths, or current susceptibilities,[54] have been computed for the C≡C, or B≡N bonds of the reacting acetylene and iminoborane molecules and for the new forming C···C bonds of benzene and planar COT and B···N bonds of borazine. The bond current strength is perhaps one of the best magnetic quantifiers of aromaticity available.[20] Differently from other currently used magnetotropicity quantifiers such as magnetic susceptibility exaltation,[55,56] out-of-plane magnetizability and magnetizability anisotropy,[57] and nucleus-independent chemical shift (NICS),[58] the bond current strength does not depend explicitly on any geometrical parameter, such as the area or radius of the ring current.[59] Each bond current strength has been computed as the integral of the current density cross section over a plane bisecting the bond taken into account. Typically, such a cross section (for π-electrons) presents two maxima and two minima disposed as symmetric pairs above and below the molecular plane. Then, integration domains were chosen to be those plane portions included within contour level at $+/-10^{-6}$ a.u. containing one maximum/minimum of the current density cross section, i.e., there are four integration domains for each bond.[52] In the following Tables, symmetric contributions to bond current strengths have been summed together; then, for each bond, two are the current strengths reported, one positive I^{Exter} for the external side of the bond with respect to the ring, and one negative I^{Inter} for the internal side of the bond. The sum $I = I^{\mathrm{Exter}} + I^{\mathrm{Inter}}$ is also reported. We remark that for the purpose of this work it is more convenient to use an unsigned current strength, at difference with that defined elsewhere.[14]

3 Sum of vortices

In this section we outline a simple mathematical model for the sum of noninteracting two-dimensional vortical fields, which will be useful to explain and discuss a number of features of the current density induced by a magnetic field in the π-electronic cloud of the molecules taken into account. The model extends the study of the sum of two planar purely rotational fields (PRF), presented previously,[30] to the sum of three or more PRFs. Then, adopting the same definition as before, we assume an hypothetical planar PRF as $\mathbf{J} = J_\theta \hat{\theta}$, where $J_\theta = J_\theta(r)$ is a somewhat arbitrary function profile that vanishes in the centre ($r = 0$) and at infinity and reaches a maximum value at $r_{\max}$, see bottom of Fig. 1 for an example. For the sake of simplicity, hereafter $J(r) \equiv J_\theta(r)$. Despite the simplicity of such a PRF, a free disposition of a number of them over a plane, with different $J(r)$ and tropicity, leads to a rather complex problem. Since our aim is to develop, as far as possible, the model analytically, some simplification has to be done. We consider then only sum of vortices disposed in the plane at the corners of regular polygons. Moreover, according to the purposes of the present work, a further simplification comes from the requirement that all vortices shall have the same shape and tropicity, i.e. they are all described by the same $J(r)$ and all rotate the same way either clockwise or counter-clockwise.
The field resulting from the sum of PRFs can be analysed determining its critical points and phase portrait. Therefore, the analysis will be carried out looking for such critical points and working out the phase portrait.

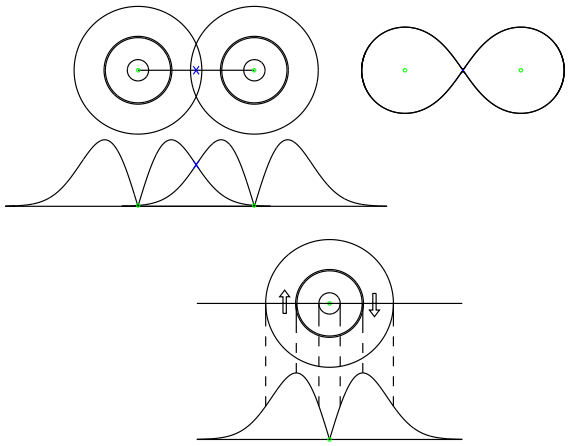

Fig. 1 Bottom: a planar PRF, with $J(r)$ given by eq. 9, is represented by means of three circular trajectories and a profile of $|\mathbf{J}|$ along a diameter. The circular trajectories are for $|\mathbf{J}|_{\max} = J(r_{\max})$ (bold circle) and for $|\mathbf{J}| = 0.5|\mathbf{J}|_{\max}$ (the two thinner circles aside). Top: the superposition of two identical and homotropic PRFs, spaced by $3.5r_{\max}$, is shown on the left; the phase portrait of the resultant field is shown on the right. Critical points, where the total field is vanishing, are marked as follows: small green/red circles are centres of clockwise/anti-clockwise vortices; blue crosses represent saddles.

We have shown that summing two PRFs the critical points can only be found along the straight line that connects their centres and that the nature of these critical points is determined by the slopes of the $|J(r)|$ functions. For the particular case shown on top of Fig. 1, where two identical and homotropic PRFs are set apart at a distance greater than $2r_{\max}$, three critical points characterize the resulting field in the inner region. These are: two centres close to the original ones, since the larger slope of the two $|J(r)|$ functions, i.e., the dominating one, is increasing; and a saddle, exactly placed in the middle, since both slopes are decreasing.[30] As clearly shown by the phase portrait on the right of Fig. 1, the resulting field can be described as formed by two regions of local circulation that are enclosed within an external delocalised one. This representation, in particular, has revealed quite useful to rationalize the current density induced by a magnetic field perpendicular to the H-bonds[28] and H-H bonds.[29] Getting the two PRFs even closer, the two centres move toward the central saddle, until they merge together to form a single vortex that has the

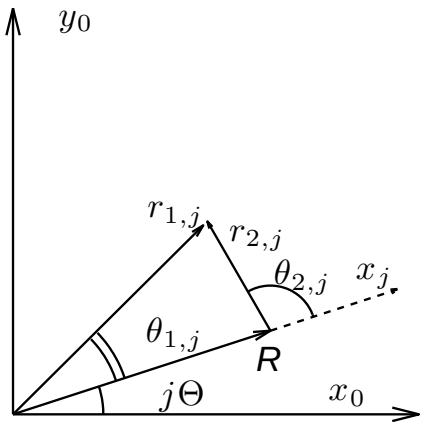

Fig. 2 Geometric parameters of the models of sum of N PRFs.

same tropicity of the original PRFs. This happens when the maxima of the two $|J(r)|$ functions are superimposed, i.e., when the PRFs are $2r_{\max}$ far apart.[30]

3.1 Sum of N PRFs

Now, let us develop the model for the sum of three or more PRFs placed in the xy plane, centreed at a distance R from the origin and arranged according to C_{Nh} symmetry. Parent fields will be numbered from 0 to $N-1$, i.e. $J^{(0)}(r_0)$, $J^{(1)}(r_1)$, $\ldots J^{(N-1)}(r_{N-1})$, or, considering the assumption of equal vortices, $J^{(0)}(r_0)$, $J^{(0)}(r_1)$, $\ldots J^{(0)}(r_{N-1})$. Vortex 0 will be on the positive x axis. The current density generated by the j-th vortex in the centre has been previously determined for a Cartesian coordinate system with axis x_j pointing from the origin to the j-th vertex and is

$$\begin{bmatrix} J_{x_j} \\ J_{y_j} \end{bmatrix} = \begin{bmatrix} -\frac{r_{1,j}\sin\theta_{1,j}}{r_{2,j}} \\ \frac{r_{1,j}\cos\theta_{1,j}-R}{r_{2,j}} \end{bmatrix} J^{(0)}(r_{2,j}), \tag{4}$$

where $r_{2,j}=\sqrt{r_{1,j}^2+R^2-2r_{1,j}R\cos\theta_{1,j}}$.[30] Adding up all parent fields and expressing them in a common frame with Cartesian coordinates $(x,y)\equiv(x_0,y_0)$, and polar coordinates $(r,\theta)\equiv(r_{1,0},\theta_{1,0})$, we have

$$\begin{aligned}\begin{bmatrix} J_x \\ J_y \end{bmatrix} &= \sum_{j=0}^{N-1}\begin{bmatrix} \cos j\Theta & -\sin j\Theta \\ \sin j\Theta & \cos j\Theta \end{bmatrix}\begin{bmatrix} -\frac{r\sin\theta_{1,j}}{r_{2,j}} \\ \frac{r\cos\theta_{1,j}-R}{r_{2,j}} \end{bmatrix} J^{(0)}(r_{2,j}) \\ &= \sum_{j=0}^{N-1}\begin{bmatrix} -\frac{r\sin\theta}{r_{2,j}}-\frac{R}{r_{2,j}}\sin j\Theta \\ \frac{r\cos\theta}{r_{2,j}}-\frac{R}{r_{2,j}}\cos j\Theta \end{bmatrix} J^{(0)}(r_{2,j}),\end{aligned}$$

where $\Theta=\frac{2\pi}{N}$, and $\theta=\theta_{1,j}+j\Theta$ (Fig. 2). Along the x axis $J_x=0$ because $\sin\theta=0$ and $\sin(j\Theta)=-\sin[(N-j)\Theta]$. Moreover, as $\sum_{j=0}^{N-1}\cos j\Theta=0$, the centre can be identified as a critical point. To define the nature of this point, we take the Jacobian at the origin $(\nabla\mathbf{J})_0$. Considering that for $f=f(r,\theta)$,

$$\left(\frac{\partial f}{\partial x}\right)_0=\lim_{r\to0}\frac{\partial(f)_{\theta=0}}{\partial r}$$

and

$$\left(\frac{\partial f}{\partial y}\right)_0=\lim_{r\to0}\frac{\partial(f)_{\theta=\pi/2}}{\partial r},$$

we have

$$\left(\frac{\partial r_{2,j}^{-1}}{\partial x}\right)_0=\frac{\cos(j\Theta)}{R^2},\qquad \left(\frac{\partial r_{2,j}^{-1}}{\partial y}\right)_0=\frac{\sin(j\Theta)}{R^2}$$

$$\left(\frac{\partial r_{2,j}}{\partial x}\right)_0=-\cos(j\Theta),\qquad \left(\frac{\partial r_{2,j}}{\partial y}\right)_0=-\sin(j\Theta).$$

These relations allow obtaining

$$\begin{aligned}(\nabla\mathbf{J})_0 &= \begin{bmatrix} \left(\frac{\partial J_x}{\partial x}\right)_0 & \left(\frac{\partial J_x}{\partial y}\right)_0 \\ \left(\frac{\partial J_y}{\partial x}\right)_0 & \left(\frac{\partial Jy}{\partial y}\right)_0 \end{bmatrix} \\ &= \frac{1}{R}\sum_{j=0}^{N-1}\begin{bmatrix} -\sin j\Theta\cos j\Theta & \sin^2 j\Theta-1 \\ 1-\cos^2 j\Theta & -\sin j\Theta\cos j\Theta \end{bmatrix} J^{(0)}(R)+ \\ &+ \sum_{j=0}^{N-1}\begin{bmatrix} -\sin j\Theta\cos j\Theta & \sin^2 j\Theta \\ \cos^2 j\Theta & \sin j\Theta\cos j\Theta \end{bmatrix}\left(\frac{\partial J^{(0)}(r)}{\partial r}\right)_{r=R}.\end{aligned}$$

Considering now that $\sum_{j=0}^{N-1}\sin j\Theta\cos j\Theta=\frac{1}{2}\sum_{j=0}^{N-1}\sin 2j\Theta=0$ and $\sum_{j=0}^{N-1}\cos^2 j\Theta=\sum_{j=0}^{N-1}\left(\frac{\exp(ij\Theta)-\exp(-ij\Theta)}{2}\right)^2=\frac{N}{2}(1+\delta_{N2})$, where δ_{N2} is the Krönecker symbol, we get for $N=2$

$$(\nabla\mathbf{J})_0=\begin{bmatrix} 0 & -\frac{2J^{(0)}(R)}{R} \\ 2\left(\frac{\partial J^{(0)}}{\partial r}\right)_{r=R} & 0 \end{bmatrix}, \tag{5}$$

with eigenvalues $\lambda=\pm\sqrt{-4\frac{J^{(0)}(R)}{R}\left(\frac{\partial J^{(0)}}{\partial r}\right)_{r=R}}$: the critical point is thus a centre if $\left(\frac{\partial J^{(0)}}{\partial r}\right)_{r=R}>0$ and a saddle if $\left(\frac{\partial J^{(0)}}{\partial r}\right)_{r=R}<0$. For $N>2$

$$(\nabla\mathbf{J})_0=\begin{bmatrix} 0 & -\frac{N}{2}\left[\frac{J^{(0)}(R)}{R}+\left(\frac{\partial J^{(0)}}{\partial r}\right)_{r=R}\right] \\ \frac{N}{2}\left[\frac{J^{(0)}(R)}{R}+\left(\frac{\partial J^{(0)}}{\partial r}\right)_{r=R}\right] & 0 \end{bmatrix}, \tag{6}$$

The eigenvalues of the Jacobian are therefore $\lambda=\pm i\frac{N}{2}\left[\frac{J^{(0)}(R)}{R}+\left(\frac{\partial J^{(0)}}{\partial r}\right)_{r=R}\right]$ and the critical point is always a centre. The tropicity at that centre can be obtained from the vorticity

$$(\nabla\times\mathbf{J})_{z0}=N\left[\frac{J^{(0)}(R)}{R}+\left(\frac{\partial J^{(0)}}{\partial r}\right)_{r=R}\right], \tag{7}$$

and it can be seen that the nature of the central critical point depends upon both the value of the function and its derivative. Further information can be obtained using a given functional form for $J^{(0)}$. A simple choice is

$$J^{(0)}(r)=\frac{I^{(0)}}{I_n(a)}r^n\exp(-ar^2), \tag{8}$$

where $I^{(0)}$ is the current strength of the isolated vortex, $I_n(a)$ is a Gaussian integral, and the exponent a determines the position $r_{\max}=\sqrt{\frac{n}{2a}}$ of the maximum current. Use of 8 in 7, and introduction of the side of the polygon $L=2R\sin(\pi/N)$, shows that in the

middle of the polygon there will be a heterotropic (homotropic) centre for L larger (smaller) than $2r_{\max}\sqrt{(1+\frac{1}{n})\sin\frac{\pi}{N}}$.
To further illustrate the analytical model we have considered the sum of three and four homotropic PRFs, having the $J^{(0)}(r)$ function of form 8 with $n=1$, i.e.

$$J^{(0)}(r) = I^{(0)}\frac{r}{r_{\max}}\exp\left[-\frac{1}{2}\left(\frac{r}{r_{\max}}\right)^2\right]. \quad (9)$$

We find that four homotropic vortices merge in a single vortex for $L < 2r_{\max}$, i.e. the same condition found for two vortices, while three vortices merge before the two vortices and five or more vortices merge after them. The nature of the critical points found for 3 and 4 vortices along the x axis, i.e. in the direction of a polygon radius, are shown in Figs. 3 and 4. Notably, the Figure for $N=3$ shows a small interval of distances of homotropic vortices separated by a saddle, giving rise to a characteristic phase portrait resembling a small propeller (top centre of Fig. 3).
All of these are rather intriguing facts, since they permit to infer the presence of a ring current –which we term ring current from the sum of vortices (RCSV)– only on account of the simple sum of non-interacting local vortices. Then, the following interesting question can be posed: how big is the RCSV in comparison to the conventional ring current of aromatic and anti-aromatic systems? In order to ask to this question, it is necessary to find out a way to estimate the magnitude of the RCSV. This is presented and discussed within the following section.

4 Results and discussion

Chemical reactions 1-3 have been monitored from certain RC initial values, for virtually non interacting acetylene or iminoborane molecules, to the RC final values for the equilibrium geometry of the final products, in step of 0.05 Å. We remark that, according to its definition, RC coincides with the distance R of the model. Some further finer steps have been taken to better describe the current density evolution. The sorted full set of current density maps of each chemical reaction has been collected into an animation available within the ESI. Each animation frame reports the C≡C (or B≡N) bond current strengths of the approaching units and the C···C (or B···N) current strengths of the forming bonds, separated into external and internal contributions, along with the RC value. Taking a look of the animations is, therefore, recommended for the completeness of the information that can be retrieved. Here, a selection of the most informative frames is presented for benzene, planar COT, and borazine, but let's start estimating the RCSV.

4.1 DFT estimates of the RCSV

To estimate the RCSV, we have taken the equilibrium geometries of benzene and planar COT and have separated them in three and four distorted acetylene units. Similarly, we have cut out three distorted iminoborane (BH_2N) molecules from the equilibrium geometry of borazine. Then, for each single distorted acetylene and iminoborane molecule, we have computed the π-orbital contribution to the current density induced by a perpendicular magnetic field at DFT level, as described in the previous

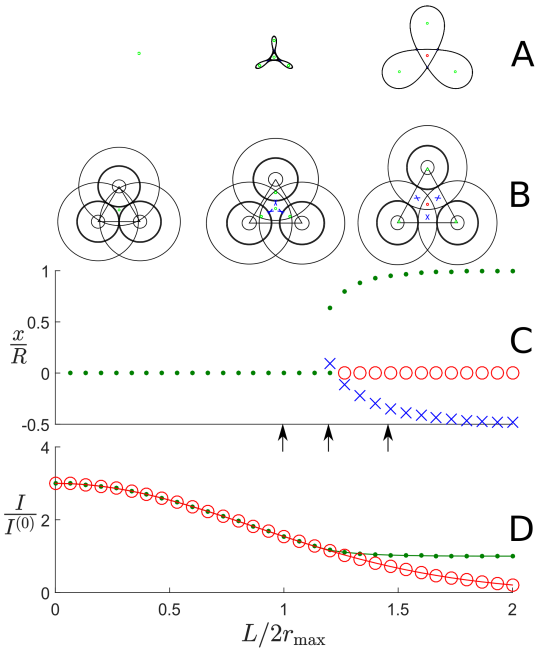

Fig. 3 Topological features of the vectorial field obtained by the sum of 3 PRFs defined by eq. 9; the origins of the 3 PRFs are at the vertices of regular triangles of radius R and side L. The nature of the critical points along the vertical x axis is graphically reported in C: saddles, homotropic and heterotropic centres are marked with ×, • and o, respectively. The sets of all the critical points occurring for the three representative distances marked with arrows are reported in A and B. In A the separatrices are added to show the phase portrait; in B each of the 3 parent PRFs is depicted by three representative trajectories as in Fig. 1. In D lines with small green dots give the current density strength computed on the external side of the outer homotropic centre; lines with red circles give the current strength computed on the whole half-plane ($x \geq 0$).

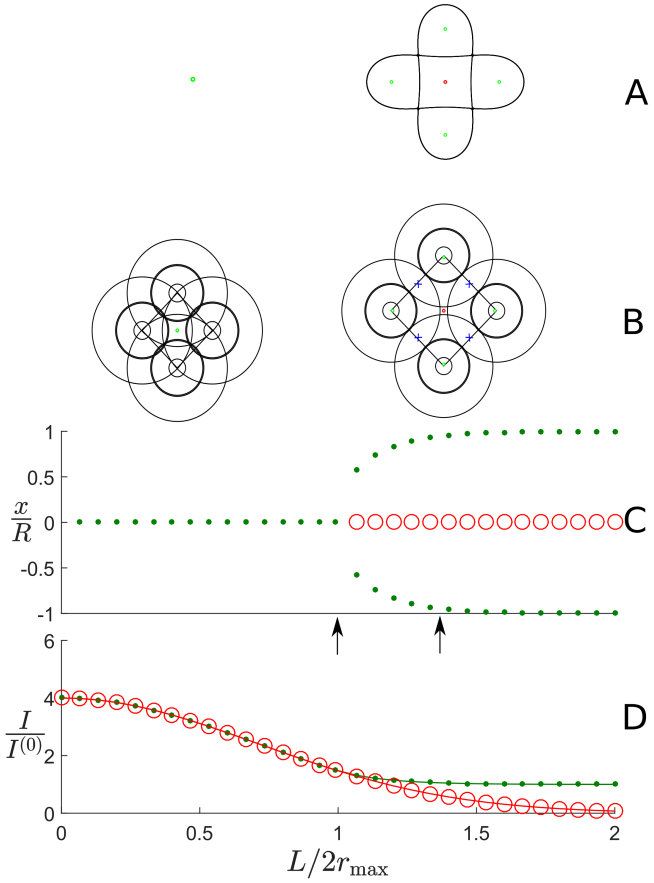

Fig. 4 Topological features of the vectorial field obtained by the sum of 4 PRFs defined by eq. 9; the origins of the 4 PRFs are at the vertices of squares of radius R and side L. For plotting details see the caption of Figure 3.

section. Finally, we have taken the sum of these individual current density fields to reconstruct the benzene, planar COT, and borazine molecules in a Kekulé-like shape. Maps of aggregated current densities at 1 a.u. above the molecular planes are shown in Fig. 5. Encouraging enough, the maps in Fig. 5 are quite in agreement with those predicted by the simplified mathematical model, suggesting that the form of rotational fields is not fundamental to predict the circulation regimes. In particular, the critical points, their nature and positions and phase portraits are in satisfactorily concordance with their analogues of Figs. 3 and 4. Then, the magnitude of the diatropic RCSV, observed in the current density maps of Fig. 5, has been evaluated by computing the C≡C and B≡N bond current strengths.[54] Their values, compared to the current strengths of distorted, isolated acetylene and iminoborane molecules, are collected in Table 1. Bond current

Table 1 π-electron contributions to the C≡C and B≡N bond current strengths in nA T^{-1} for the hypothetical Kekulé-like benzene, borazine, and planar COT molecules

Molecule	I^{Exter}	I^{Inter}	I
Benzene	3.40	−2.63	0.77
Borazine	2.63	−2.10	0.53
planar COT	3.50	−3.32	0.18
distorted C_2H_2 as in benzene	3.39	−3.27	0.12
distorted C_2H_2 as in COT	3.50	−3.39	0.12
distorted BH_2N as in borazine	2.62	−2.66	−0.04

strengths for the external/internal domains are reported under the heading Exter/Inter, assuming the positive/negative sign for external/internal cross sections. Since the acetylene units forming benzene and planar COT are differently distorted, two values are given for them. The sum of external and internal contributions reported in the last column is the measure of the RCSV magnitude that we were looking for. In practical calculation the divergence of the current density field is not vanishing everywhere, therefore the total bond current strengths for individual acetylene and iminoborane molecules is not exactly zero as it should be. Then, the last three total values give an idea of the intrinsic error affecting our estimates, which we guess to be about 0.1 nA T^{-1}. Considering the bond current strengths reported in literature and those reported here in the following, the RCSV is only a minimal part of the π-electron ring current of such systems. At any rate, for benzene a value of 0.8±0.1 nA T^{-1} should be taken as a correction of the accepted value, if the ring current strength is to be considered an emerging property not already present in the parent units. For planar COT the RCSV contribution is not significant. Approximatively one fifth of the weak diatropic ring current of borazine is due to the sum of local vortices.

4.2 Benzene

Current density maps, bond lengths, and bond current strengths for selected RC values of the hypothetical concerted trimerization of acetylene to benzene are reported in Fig. 6 and Table 2. More values and energies can be found in the ESI.

At the chosen starting RC value of 2.00 Å, the three reacting acetylene molecules interact very a little. In fact, bond lengths and angles are very similar to those of the isolated molecules and the

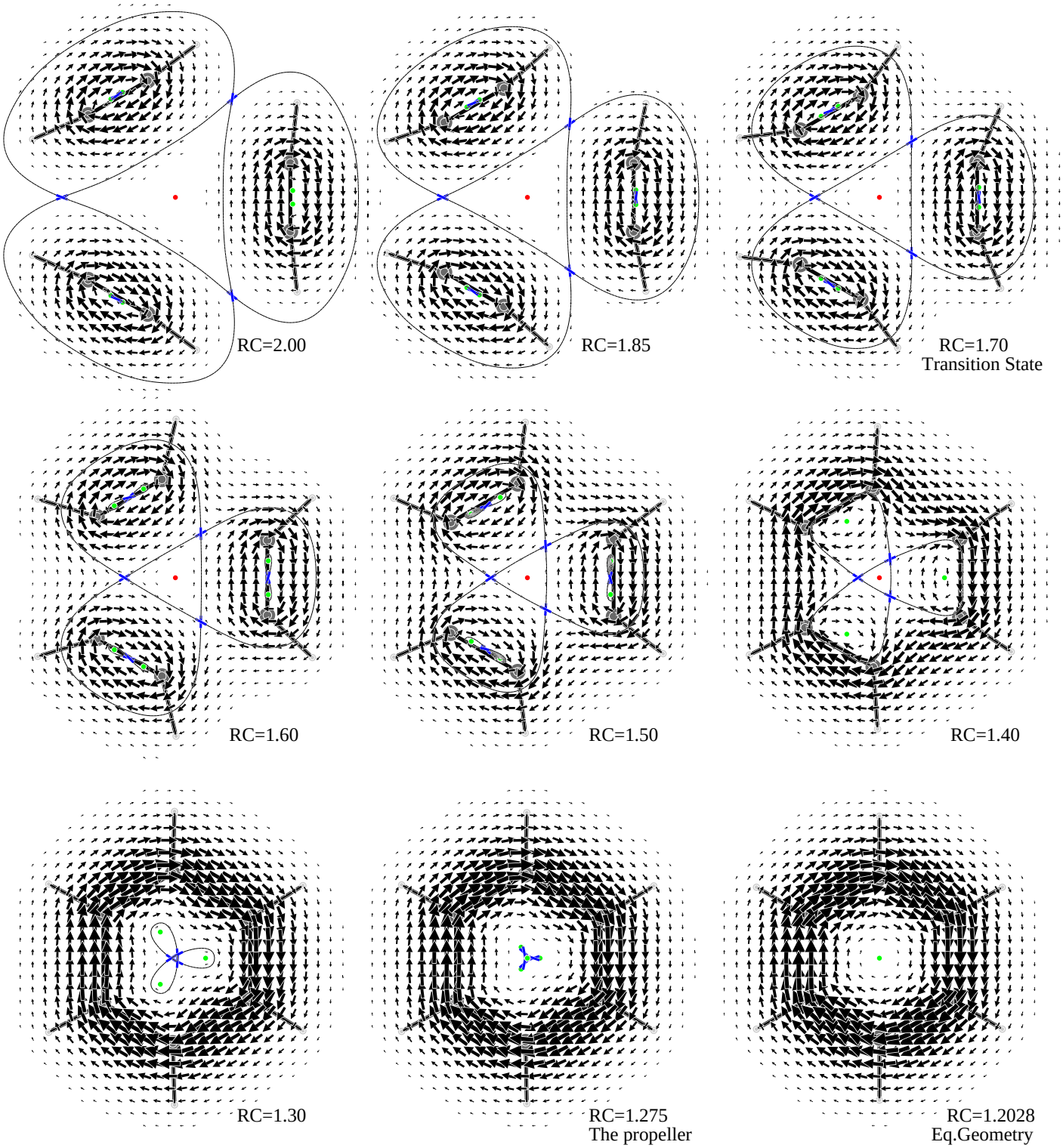

Fig. 6 A selection of frames for the hypothetical concerted trimerization of acetylene to benzene, showing the evolution of the π-electron current density induced by a perpendicular magnetic field, on a plane placed 1 a.u. above the molecular plane. Saddle points of the current density field are marked with blue crosses; the position of diatropic/paratropic centres is indicated with green/red dots. Black lines asymptotic to saddles form the phase portrait of the current density. The value of the reaction coordinate (RC) is given to the side of each map.

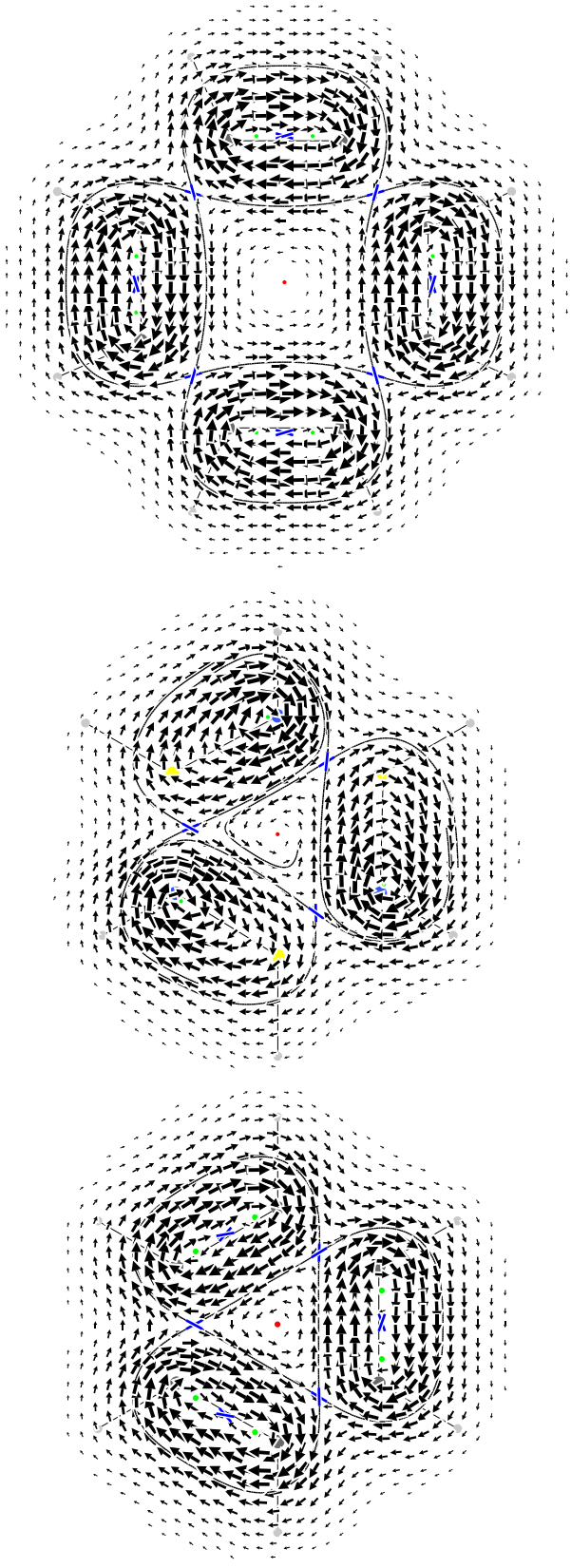

Fig. 5 Sum of current densities induced in the π-electron cloud by a perpendicular magnetic field at 1 a.u. above the molecular plane of distorted acetylene and iminoborane (BH_2N) molecules, disposed as to fit the structure of benzene (bottom), borazine (middle), and planar COT (top). Diatropic/paratropic vortices are clockwise/counter-clockwise.

Table 2 Optimized bond lengths in Å and bond current strengths I in nA T^{-1} for the frames in Fig. 6 of the trimerization reaction of acetylene to benzene. The reaction coordinate RC is in Å

RC	$r_{C\equiv C}$	$r_{C\cdots C}$	$I^{Exter}_{C\equiv C}$	$I^{Inter}_{C\equiv C}$	$I_{C\equiv C}$	$I^{Exter}_{C\cdots C}$	$I^{Inter}_{C\cdots C}$	$I_{C\cdots C}$
2.000	1.195	2.867	3.7	−3.5	0.1	0.2	−0.1	0.1
1.850	1.196	2.606	3.7	−3.5	0.2	0.2	−0.2	0.1
1.700	1.213	2.338	3.7	−3.3	0.5	0.4	−0.2	0.2
1.600	1.303	2.120	3.8	−2.8	1.0	0.9	−0.2	0.7
1.500	1.343	1.926	4.4	−2.0	2.3	2.3	−0.1	2.2
1.400	1.370	1.740	6.2	−0.8	5.4	5.3	−0.0	5.3
1.300	1.394	1.555	9.9	−0.0	9.9	9.8	−0.0	9.8
1.275	1.398	1.510	10.8	−0.0	10.8	10.7	0.0	10.7
1.203	1.389	1.389	11.8		11.8	11.8		11.8

energy is almost equal to three times the energy of one acetylene molecule. However, some distinctive features of the current density map, at this RC initial value, show that the sum of vortices is already effective, see the three saddle points and the central paratropic centre in the upper left corner frame of Fig. 6. Nonetheless, the phase portrait clearly shows circumscribed acetylene vortices, whilst the delocalised current is not appreciable, even in quantitative terms, as shown by the vanishing $I_{C\equiv C}$ and $I_{C\cdots C}$ values reported in the first row of Table 2.

According to the simplified model, as the reaction proceeds saddles points come closer restricting the central paratropic area. It is interesting to note that this topological structure can be appreciated well beyond the transition state of the reaction, which we guess at about RC=1.70 Å, where the energy of the whole system approaches its maximum value. Step by step, the external delocalised circulation grows, as documented also by the tabulated current strengths. It is worth noting that $I_{C\equiv C}$ and $I_{C\cdots C}$ values are always very close one to each other, documenting that our estimates satisfy the current continuity constrain to a very good extent. At RC=1.40 Å, it is already evident that the current flowing within the external domain of the phase portrait, will become the diatropic benzene ring current. At this point, the current strength is about half of the final value. The increasing electron sharing between acetylene units, during the concerted reaction, has the effect to enlarge the vortices as can be seen in the second to last frame of Fig. 6, and when RC=1.275 Å, the very peculiar propeller shape of the phase portrait predicted by the model can actually be observed. Remarkably, an almost complete diatropic ring current is flowing even before bond equivalence. The values in the second and third to last rows of Table 2 show that when the C≡C and C···C bond lengths are in the range of formal double and single CC bond respectively, i.e., when the aromatic electron delocalisation is not yet accomplished, the ring current strength reach 83-91% of its final value.

The positions of the critical points along the x axis of benzene as obtained from the DFT calculations (Fig. 7, top) match semiquantitatively the results expected from the model. Nicely enough, the centre-saddle-centre linear pattern predicted by the model at $L/(2r_{max}) = 1.2$ is also obtained in the DFT map for $L/2 = 1.10$ Å, giving an effective $r_{max} = 1.10/1.2$ Å $= 0.92$ Å. The most relevant difference between model prediction and the DFT results is the location of saddles at large distances: in the model the asymptotic location of the saddle is at $x/R = -1$, while from the DFT

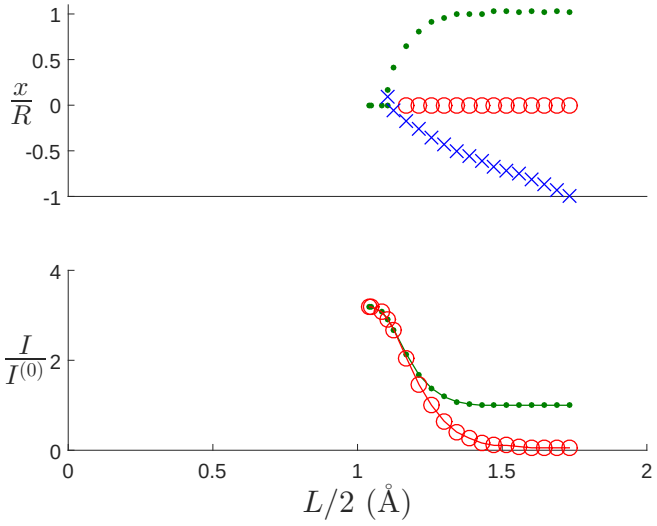

Fig. 7 Critical points (top) and current strengths (bottom) found on the x axis for the current density field obtained from the DFT calculations used to study the trimerization reaction of benzene. L (the side of the triangle) is the distance of the C≡C midpoints of the parent acetylene molecules. Saddles, diatropic and paratropic centres are marked with ×, • and o, respectively. In the bottom panel, lines with small green dots (red circles) give $I^{\text{Exter}}_{\text{C}\equiv\text{C}}$ ($I_{\text{C}\equiv\text{C}}$), divided by the current strength of the isolated acetylene molecule (3.7 nA T^{-1})

calculation that location is at $x/R = -2$. This difference is readily understood considering that individual acetylene molecules are to be considered as summations of two vortices centreed on C atoms rather than single vortices placed in the middle of the C≡C bond, as can be seen in the current density maps. Minor differences are observed for the location of the diatropic centre, which in the DFT calculations can slightly exceed the triangle radius R. This deviation from the model can be understood as a perturbation caused by the bending of the C−H bonds of the acetylene molecules. Coming to the current strengths, if they are normalized to the acetylene bond current strength obtained at large distances (3.7 nA T^{-1}), it can be seen that at the equilibrium geometry the maximum normalized current strength (3.19) slightly exceed the maximum value 3 expected for a sum of PRFs of fixed strength $I^{(0)}$. This observation suggests a picture of three parent vortices whose intensity undergoes a strengthening as the distance among them decreases. A more quantitative idea of this strengthening can be obtained by comparison of the Figs. 3 and 7. Values for r_{max} can be obtained by comparison of the location of the diatropic centres in the DFT maps with those predicted by the model; r_{max} turns out to increase from 0.76 to 0.97 Å, while the side L of the triangle formed by the midpoints of the acetylene bonds lowers from 2.7 to 2.35 Å. Use of these values of r_{max} in the curve for the delocalised current of the model, together with the DFT values for it, give a value of $I^{(0)}$ increasing from 3.6 to 6.7 nA T^{-1} upon the same reduction of distances.

4.3 Planar cyclooctatetraene

Current density maps, bond lengths, and bond current strengths for selected RC values of the hypothetical concerted tetramerization of acetylene to planar COT are reported in Fig. 8 and Table 3. More values and energies can be found in the ESI.

Table 3 Optimized bond lengths in Å and bond current strengths in nA T^{-1} for the frames in Fig. 8 of the tetramerization reaction of acetylene to planar COT. The reaction coordinate RC is in Å

RC	$r_{\text{C}\equiv\text{C}}$	$r_{\text{C}\cdots\text{C}}$	$I^{\text{Exter}}_{\text{C}\equiv\text{C}}$	$I^{\text{Inter}}_{\text{C}\equiv\text{C}}$	$I_{\text{C}\equiv\text{C}}$	$I^{\text{Exter}}_{\text{C}\cdots\text{C}}$	$I^{\text{Inter}}_{\text{C}\cdots\text{C}}$	$I_{\text{C}\cdots\text{C}}$
2.600	1.191	2.835	3.6	−3.7	−0.1	0.1	−0.2	−0.2
2.500	1.191	2.694	3.5	−3.7	−0.1	0.1	−0.3	−0.2
2.350	1.316	2.393	3.3	−3.5	−0.2	0.2	−0.4	−0.3
2.200	1.345	2.160	3.2	−3.4	−0.2	0.2	−0.6	−0.4
2.050	1.371	1.930	2.6	−4.0	−1.3	0.1	−1.7	−1.6
1.950	1.380	1.782	1.6	−5.7	−4.1	0.0	−4.4	−4.4
1.850	1.376	1.643	0.4	−11.6	−11.1		−11.4	−11.4
1.775	1.361	1.548	0.1	−22.0	−21.9		−22.2	−22.2
1.708	1.338	1.469		−39.4	−39.4		−39.7	−39.7

We choose an initial RC value of 2.60 Å, at which the acetylene molecules can be considered almost isolated, see also the total bond current strengths in the first row of Table 3. At this distance, the frame in the upper left corner of Fig. 8 shows four local vortices separated by four saddles and a central paratropic centre, in agreement with the simplified model of the sum of vortices. During the first reaction steps saddles approach one to another, whilst diatropic centres remain very close to the acetylene middle points. This description persists up to RC=2.20 Å, where saddles stop moving toward the system centre and invert their apparent motion, getting more distant as RC decreases. From this point on, the simplified model, elaborated for the sum of homotropic vortices, does not work any more. This can be understood considering the decomposition of the current density in orbital contributions.[23,24] In both benzene and COT the HOMO-LUMO transition is responsible for almost all of the ring current, either diatropic or paratropic. In benzene that ring current has the same tropicity of the isolated vortices at the start of the formation reaction, and its onset can be mapped on a graph like that of panel D of Fig. 3. For COT, instead, it is the paratropic contribution to become larger throughout the formation reaction, and it dominates over the diatropic vortices since RC=1.95 Å. Therefore the resultant ring current is heterotropic with respect to the parent diatropic vortices, a situation which is not considered by the model and is indeed out of the axes of panel D of Fig. 3. In a sense, the fact that the model works only for a bit of the planar cyclooctatetraene formation reaction, and that the magnetic response is afterwords located out of the axes drawn for the additivity model is distinctive of the anti-aromatic magnetic response. Returning to Fig. 8, one can see that the phase portraits permits to discern some local vortices around the approaching acetylene units up to RC=1.85 Å, step at which the paratropic ring current magnitude is already as large as 11.4 nA T^{-1}, i.e., as strong as the benzene ring current. It is worth noting in the last row of Table 3 that a ring current of about 40 nA T^{-1} is sustained at an equilibrium geometry with alternating bond lengths, i.e., a large electron delocalisation is not required for having a very strong ring current.[35,45] The current continuity requirement is nicely fulfilled.

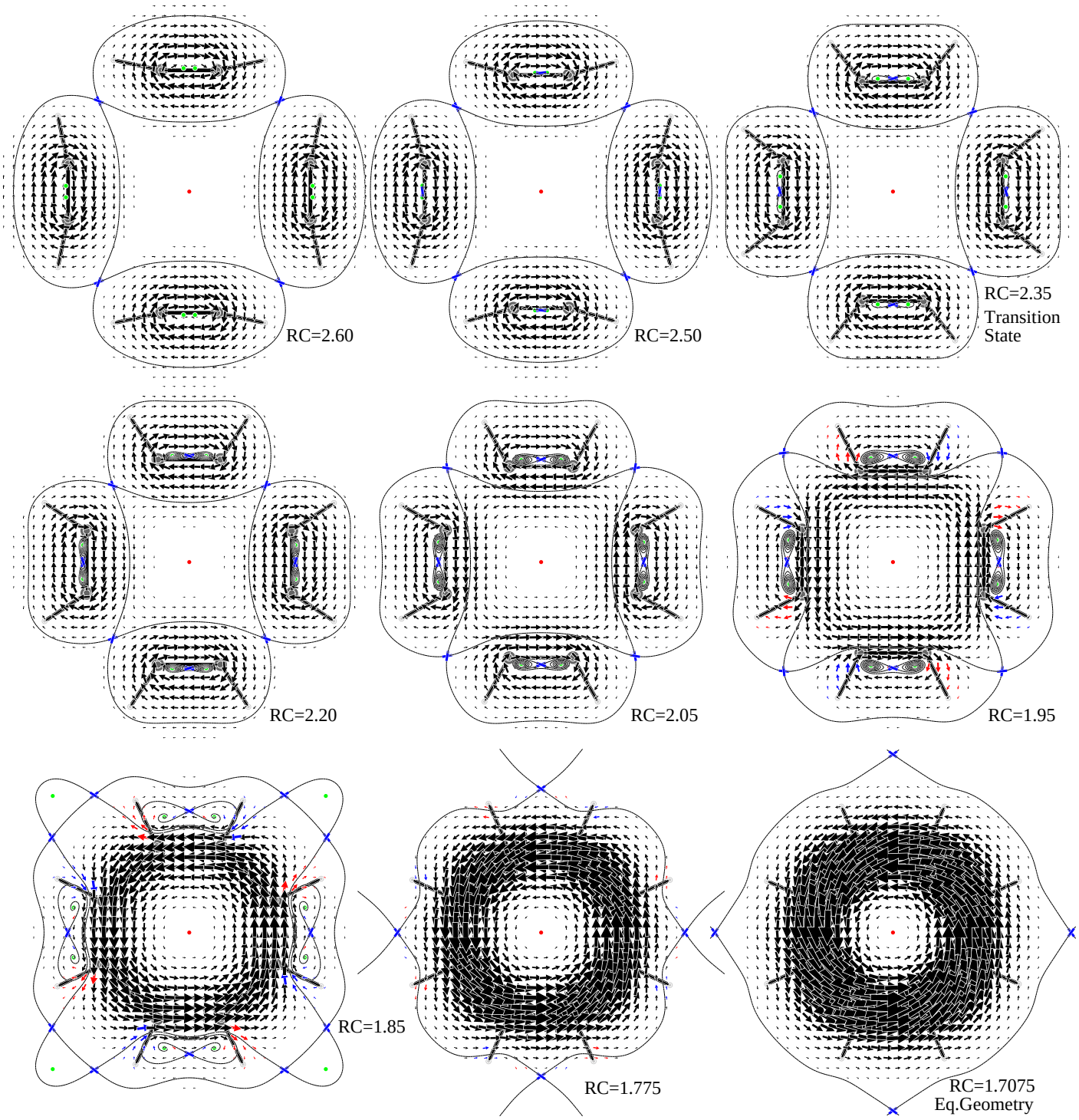

Fig. 8 A selection of frames for the hypothetical concerted tetramerization of acetylene to planar COT. For details see the caption of Fig. 6.

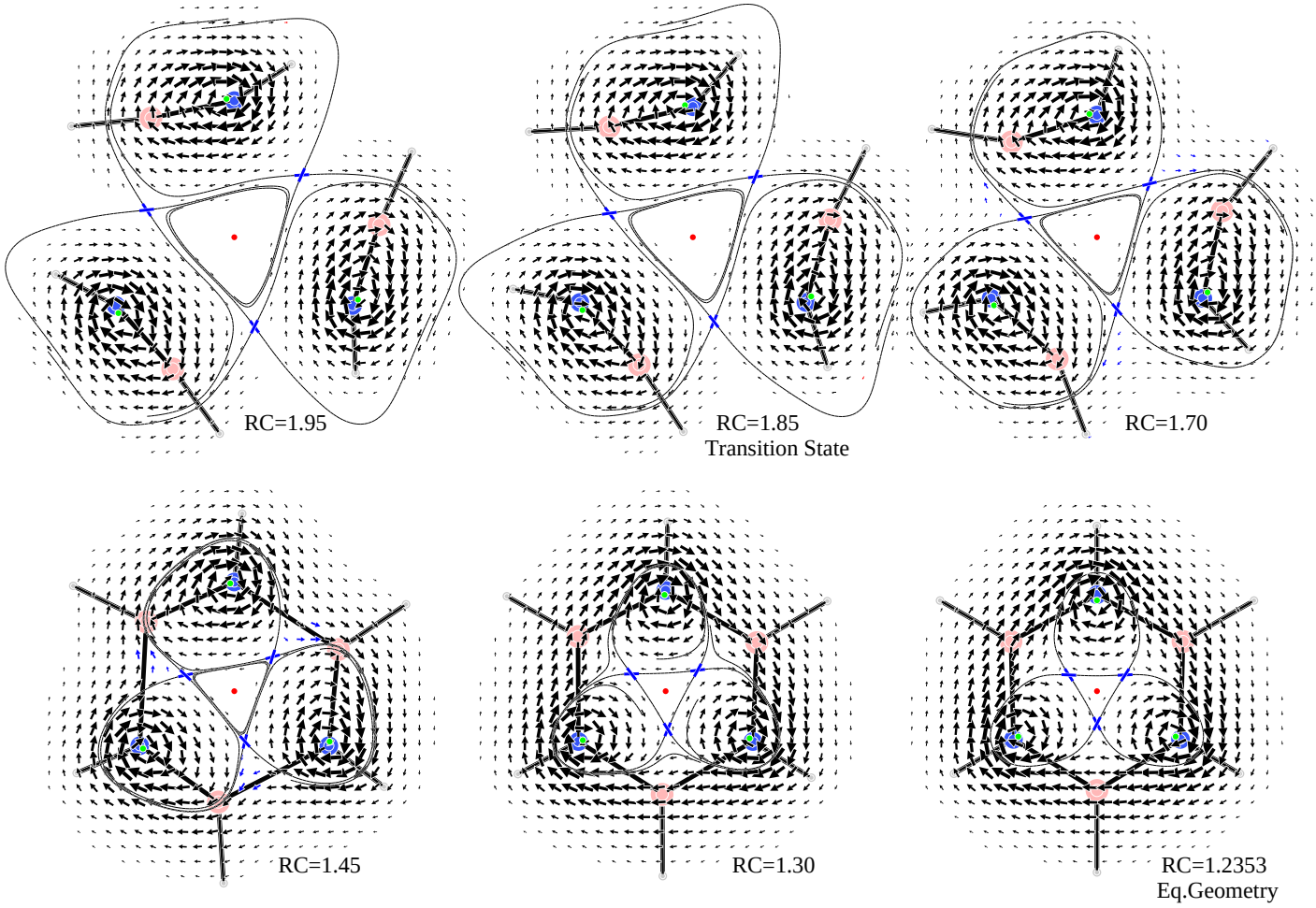

Fig. 9 A selection of frames for the hypothetical concerted trimerization of BH_2N to borazine. For details see the caption of Fig. 6.

4.4 Borazine

Current density maps, bond lengths, and bond current strengths for selected RC values of the hypothetical concerted triamerization of iminoborane BH_2N to borazine are reported in Fig. 9 and Table 4. More values and energies can be found in the ESI.

Table 4 Optimized bond lengths in Å and bond current strengths in nA T^{-1} for the frames in Fig. 9 of the trimerization reaction of BH_2N to borazine. The reaction coordinate RC is in Å

RC	$r_{B\equiv N}$	$r_{B\cdots N}$	$I^{Exter}_{B\equiv N}$	$I^{Inter}_{B\equiv N}$	$I_{B\equiv N}$	$I^{Exter}_{B\cdots N}$	$I^{Inter}_{B\cdots N}$	$I_{B\cdots N}$
1.950	1.241	2.781	2.9	−2.8	0.1	0.2	−0.1	0.1
1.850	1.257	2.595	2.8	−2.7	0.1	0.2	−0.1	0.1
1.700	1.307	2.300	2.8	−2.5	0.2	0.4	−0.2	0.3
1.450	1.410	1.808	2.7	−1.4	1.4	1.5	−0.2	1.3
1.300	1.444	1.531	3.1	−0.5	2.6	2.8	−0.2	2.6
1.235	1.428	1.428	3.3	−0.3	3.0	3.3	−0.3	3.0

Also in this case, the RC initial value (1.95 Å) was set to have almost vanishing total bond current strengths, see first row of Table 4. The current density map in the upper left corner frame of Fig. 9 shows a typical sum of vortices, separated by three saddles with a central paratropic centre, as predicted by the simplified model. As can be noticed, vortex centres are very close to nitrogen atoms and remain still during the reaction. However, some current flows also on the boron atoms, showing that a certain amount of π-electron sharing between nitrogen and boron takes place. As the reaction proceeds saddle points get closer, but do not merge together at reaction completion. Remarkably, a weak diatropic ring current can be observed to flow in the external domain of the phase portrait well before reaction completion, i.e., before bond equivalence. For example, when RC=1.45 Å the strength of this ring current is about 1.3 nA T^{-1} (see Table 4). At the borazine equilibrium geometry, boron atoms are outside the phase portrait and an almost undisturbed ring current of 3.0 nA T^{-1} pass over them. In a sense, boron atoms act like semiconductors, permitting a π-electron ring current, four times lower then in benzene, due to the low B-N π-electron sharing.

5 Conclusions

Reports of delocalised currents originating from the summation of localised vortices[28,30] called for an investigation on the extent by which the ring current is an emerging property, rather than the result of a summation of current densities of smaller chemical components.

To this end we have first generalized the model for the sum of two purely rotational fields (PRFs) to the sum of $N \geq 3$ PRFs, having the same tropicity and shape, disposed as to form a regular polygon. The model shows a distinctive phase portrait composed by N saddles, which confine N circulation centres and delimit two delocalised circulations, a con-rotating external one and a contra-rotating internal one. This intuitive picture is valid when the vortices are well far apart. If the vortices approach each other, keeping a regular polygonal form, the phase portrait changes in a less intuitive way that depends on N and vortex shape. The simple condition reported for $N = 2$ for the onset of a single fully delocalised current, i.e. a distance of the vortices smaller than $2r_{max}$ (with r_{max} the distance of the maximum of the current density from the origin of the isolated vortex) turns out to hold also for $N = 4$, while upon putting closer the vortices, the fully delocalised current appears earlier for $N = 3$ and later for $N > 4$. Notably, for $N = 3$, before the appearance of the fully delocalised current, a very characteristic propeller-like phase portrait emerges, whereby the three saddles are rotated by 60° with respect to the large-distance phase portrait, and the central vortex is homotropic rather than heterotropic (Fig. 3A middle).

To test then the relevance of the sum of vortices for the making of the ring currents, we have selected three archetypal cyclic system (aromatic benzene, anti-aromatic planarised COT, non-aromatic borazine) and we have performed two computational experiments.

First, we have assembled a current density for the archetypal monocycles summing the current density of the three (four for COT) parent molecules kept at the geometry occurring in the stationary geometry for the monocycles (Fig. 5). The resulting current density fields give only small amounts of the fully delocalised current: the largest delocalised contribution is 0.8 nA T^{-1} for benzene, which is less than 10% of its total ring current. This result is suggestive that the ring current is indeed an emerging property, like a good indicator of aromaticity should be.

Second, we have followed the evolution of computed π-electron current densities, induced by a perpendicular magnetic field, along the reaction path for the formation of the three chosen prototypical molecules from 3 (or 4) molecules of acetylene or iminoborane (BH_2N). The computed DFT current density patterns follow the simple model at different levels. On the one hand, in the case of the anti-aromatic COT, the pattern of computed critical points is comparable to that of the model only at large distances: the outward motion of the saddles and the onset of the large heterotropic circulation cannot be accounted by the model. On the other hand, for the diatropic cycles the agreement between computed patterns and those expected by the model is much better. It is rather surprising that signatures of the three parent acetylenes are present in the patterns of the forming benzene at distances almost as short as in the equilibrium geometry. In particular, a geometry just a bit larger than the equilibrium one (RC=1.275 Å in Fig. 6), and characterized by a delocalised current of 10.8 nA T^{-1} (a single nA T^{-1} smaller than the equilibrium geometry value), has a phase portrait with the special propeller pattern found from the sum of 3 PRFs. These findings indicate that it is possible to describe the ring current of benzene as the sum of three acetylene units, formally corresponding to a single Kekulé structure.[60] Further comparisons aimed at matching DFT and model values indicate that, as compared to the isolated acetylenes, these parent acetylenes should have a broader shape (larger r_{max}) and a larger current strength (6.7 vs 3.6 nA T^{-1}). Similar changes are not needed for borazine whose ring current strength virtually matches the bond current strength of the parent iminoborane. These two cases suggest a picture of aromatic systems as those able to force parent molecules to merge more effectively while increasing their diatropicity, while non-aromatic systems are those where the formation of the molecule does not require any significant change of the parent molecules.

Acknowledgement

Financial support from the MIUR and Università di Salerno is gratefully acknowledged.

References

1 A. Kekulé, *Bull. Soc. Chim. Fr.*, 1865, **3**, 98.
2 L. Pauling, *J. Chem. Phys.*, 1936, **4**, 673.
3 K. Lonsdale, *Proceedings of the Royal Society A: Mathematical, Physical and Engineering Sciences*, 1937, **159**, 149–161.
4 F. London, *J. Phys. Radium*, 1937, **8**, 397–409.
5 E. Hückel, *Z. Phys.*, 1931, **70**, 204–286.
6 E. Hückel, *Z. Phys.*, 1931, **72**, 310–337.
7 E. Hückel, *Z. Phys.*, 1932, **76**, 628–648.
8 E. Hückel, *Z. Phys.*, 1933, **83**, 632–668.
9 Inaki Morao and Fernando P. Cossio, *J. Org. Chem.*, 1999, **64**, 1868–1874.
10 J. Jusélius and D. Sundholm, *Phys. Chem. Chem. Phys.*, 1999, **1**, 3429–3435.
11 C. Foroutan-Nejad, S. Shahbazian, F. Feixas, P. Rashidi-Ranjbar and M. Solà, *J. Comput. Chem.*, 2011, **32**, 2422–2431.
12 S. Pelloni and P. Lazzeretti, *J. Phys. Chem. A*, 2011, **115**, 4553–4557.
13 S. Pelloni and P. Lazzeretti, *J. Phys. Chem. A*, 2013, **117**, 9083–9092.
14 G. Monaco and R. Zanasi, *J. Phys. Chem. A*, 2014, **118**, 1673–1683.
15 M. Baranac-Stojanović, *RSC Adv.*, 2014, **4**, 308–321.
16 D. Du, D. Sundholm and H. Fliegl, *J. Chin. Chem. Soc.*, 2015.
17 P. Lazzeretti, *Prog. Nucl. Magn. Reson. Spectrosc.*, 2000, **36**, 1–88.
18 J. A. N. F. Gomes and R. B. Mallion, *Chem. Rev.*, 2001, **101**, 1349–1384.
19 Z. Chen, C. S. Wannere, C. Corminboeuf, R. Puchta and P. v. R. Schleyer, *Chem. Rev.*, 2005, **105**, 3842–3888.
20 H. Fliegl, S. Taubert, O. Lehtonen and D. Sundholm, *Phys. Chem. Chem. Phys.*, 2011, **13**, 20500.
21 R. Gershoni-Poranne and A. Stanger, *Chem. Soc. Rev.*, 2015, **44**, 6597–6615.
22 F. Feixas, E. Matito, J. Poater and M. SolÃă, *Chem. Soc. Rev.*, 2015, **44**, 6434–6451.
23 E. Steiner and P. W. Fowler, *J. Phys. Chem. A*, 2001, **105**, 9553–9562.
24 E. Steiner and P. W. Fowler, *Chem. Commun.*, 2001, 2220–2221.
25 A. Soncini, P. Fowler, P. Lazzeretti and R. Zanasi, *Chem. Phys. Lett.*, 2005, **401**, 164–169.
26 S. Pelloni and P. Lazzeretti, *Int. J. Quantum Chem.*, 2011, **111**, 356–367.
27 S. Pelloni, G. Monaco, P. Della Porta, R. Zanasi and P. Lazzeretti, *J. Phys. Chem. A*, 2014, **118**, 3367–3375.
28 G. Monaco, P. Della Porta, M. Jabłoński and R. Zanasi, *Phys. Chem. Chem. Phys.*, 2015, **17**, 5966–5972.
29 P. Della Porta, R. Zanasi and G. Monaco, *J. Comput. Chem.*, 2015, **36**, 707–716.
30 G. Monaco and R. Zanasi, *J. Chem. Phys.*, 2009, **131**, 044126.
31 C. A. Thompson and L. Andrews, *J. Am. Chem. Soc.*, 1995, **117**, 10125–10126.
32 P. Paetzold, *Advances in Inorganic Chemistry*, Elsevier, 1987, vol. 31, pp. 123–170.
33 R. Willstätter and E. Waser, *Ber. Dtsch. Chem. Ges.*, 1911, **44**, 3423–3445.
34 P. W. Fowler and E. Steiner, *J. Phys. Chem. A*, 1997, **101**, 1409–1413.
35 P. W. Fowler, R. W. A. Havenith, L. W. Jenneskens, A. Soncini and E. Steiner, *Angew. Chem. Int. Ed.*, 2002, **41**, 1558–1560.
36 R. Islas, E. Chamorro, J. Robles, T. Heine, J. C. Santos and G. Merino, *Struct. Chem.*, 2007, **18**, 833–839.
37 M. J. Frisch, G. W. Trucks, H. B. Schlegel, G. E. Scuseria, M. A. Robb, J. R. Cheeseman, G. Scalmani, V. Barone, B. Mennucci, G. A. Petersson, H. Nakatsuji, M. Caricato, X. Li, H. P. Hratchian, A. F. Izmaylov, J. Bloino, G. Zheng, J. L. Sonnenberg, M. Hada, M. Ehara, K. Toyota, R. Fukuda, J. Hasegawa, M. Ishida, T. Nakajima, Y. Honda, O. Kitao, H. Nakai, T. Vreven, J. A. Montgomery Jr., J. E. Peralta, F. Ogliaro, M. Bearpark, J. J. Heyd, E. Brothers, K. N. Kudin, V. N. Staroverov, T. Keith, R. Kobayashi, J. Normand, K. Raghavachari, A. Rendell, J. C. Burant, S. S. Iyengar, J. Tomasi, M. Cossi, N. Rega, J. M. Millam, M. Klene, J. E. Knox, J. B. Cross, V. Bakken, C. Adamo, J. Jaramillo, R. Gomperts, R. E. Stratmann, O. Yazyev, A. J. Austin, R. Cammi, C. Pomelli, J. W. Ochterski, R. L. Martin, K. Morokuma, V. G. Zakrzewski, G. A. Voth, P. Salvador, J. J. Dannenberg, S. Dapprich, A. D. Daniels, O. Farkas, J. B. Foresman, J. V. Ortiz, J. Cioslowski and D. J. Fox, *Gaussian 09, Revision D.01, Gaussian, Inc., Wallingford CT*, 2013.
38 P. J. Wilson, T. J. Bradley and D. J. Tozer, *J. Chem. Phys.*, 2001, **115**, 9233.
39 T. H. Dunning, *J. Chem. Phys.*, 1989, **90**, 1007.
40 T. A. Keith and R. F. Bader, *Chem. Phys. Lett.*, 1993, **210**, 223–231.
41 P. Lazzeretti, M. Malagoli and R. Zanasi, *Chem. Phys. Lett.*, 1994, **220**, 299–304.
42 S. Coriani, P. Lazzeretti, M. Malagoli and R. Zanasi, *Theor. Chim. Acta*, 1994, **89**, 181–192.
43 R. Zanasi, P. Lazzeretti, M. Malagoli and F. Piccinini, *J. Chem. Phys.*, 1995, **102**, 7150.
44 R. Zanasi, *J. Chem. Phys.*, 1996, **105**, 1460.
45 R. W. Havenith and P. W. Fowler, *Chem. Phys. Lett.*, 2007, **449**, 347–353.
46 A. Soncini, A. M. Teale, T. Helgaker, F. De Proft and D. J. Tozer, *J. Chem. Phys.*, 2008, **129**, 074101.
47 R. W. Havenith, A. J. Meijer, B. J. Irving and P. W. Fowler, *Mol. Phys.*, 2009, **107**, 2591–2600.
48 P. Lazzeretti, M. Malagoli and R. Zanasi, *Technical Report on Project "Sistemi Informatici e Calcolo Parallelo"*, CNR Research Report 1/67, 1991.

49 P. W. Fowler, E. Steiner, R. W. A. Havenith and L. W. Jenneskens, *Magn. Reson. Chem.*, 2004, **42**, S68–S78.

50 D. Flaig, M. Maurer, M. Hanni, K. Braunger, L. Kick, M. Thubauville and C. Ochsenfeld, *J. Chem. Theory Comput.*, 2014, **10**, 572–578.

51 R. M. Stevens, R. M. Pitzer and W. N. Lipscomb, *J. Chem. Phys.*, 1963, **38**, 550.

52 G. Monaco, R. Zanasi, S. Pelloni and P. Lazzeretti, *J. Chem. Theory Comput.*, 2010, **6**, 3343–3351.

53 E. A. Coddington and N. Levinson, *Theory of ordinary differential equations*, R.E. Krieger, Malabar, Fla, 1984.

54 J. Jusélius, D. Sundholm and J. Gauss, *J. Chem. Phys.*, 2004, **121**, 3952.

55 H. J. Dauben, J. D. Wilson and J. L. Laity, *J. Am. Chem. Soc.*, 1968, **90**, 811–813.

56 H. J. Dauben, J. D. Wilson and J. L. Laity, *J. Am. Chem. Soc.*, 1969, **91**, 1991–1998.

57 W. H. Flygare, *Chem. Rev.*, 1974, **74**, 653–687.

58 P. v. R. Schleyer, C. Maerker, A. Dransfeld, H. Jiao and N. J. R. v. E. Hommes, *J. Am. Chem. Soc.*, 1996, **118**, 6317–6318.

59 S. Pelloni, G. Monaco, R. Zanasi and P. Lazzeretti, *AIP Conf. Proc.*, 2012, **1456**, 114–118.

60 R. W. A. Havenith, *J. Org. Chem.*, 2006, **71**, 3559–3563.